Road grades and tire forces estimation using two-stage extended Kalman filter in a delayed interconnected cascade structure

R. Cordeiro, A. Ribeiro, J. Azinheira, A. Victorino, P. Ferreira, E. de Paiva, S. Bueno

Road Grades and Tire Forces Estimation Using Two-Stage Extended Kalman Filter in a Delayed Interconnected Cascade Structure*

R. A. Cordeiro[1], A. M. Ribeiro[2], J. R. Azinheira[2], A. C. Victorino[3], P. A. V. Ferreira[1]
E. C. de Paiva[4] and S. S. Bueno[5]

***Abstract*— Intelligent vehicles sense their dynamics and the environment to make proper decisions. Some of this information are hard to be measured or need expensive sensors. This paper addresses the estimation of road grade angles, along with tire-ground interaction forces, in a delayed interconnected cascade observer structure. A new approach using a Two-Stage Extended Kalman Filter is proposed, allowing a robust simultaneous estimation of the slow and fast dynamics variables. Experimental data is used to validate the estimator.**

NOMENCLATURE

Index $_i$:	$<$ 1 (front) | 2 (rear) $>$
Index $_j$:	$<$ 1 (left) | 2 (right) $>$
$F_{x_{ij}}$,$F_{y_{ij}}$,$F_{z_{ij}}$:	Long., lat. and vert. tire force
m:	Vehicle mass
g:	Gravitational acceleration
u,v,w:	Long., lat. and vert. linear speed
a_x,a_y,a_z:	Long., lat. and vert. acceleration
p,q,r:	Roll, pitch and yaw rate
ϕ, θ:	Roll and pitch angle
J_{xx},J_{yy},J_{zz}:	Principal inertia in each axis
L_i:	Distance from CG to front/rear.
E :	Distance from CG to lateral
k_s,c_s:	Suspension stiffness and damper coeff.
δ_{ij} :	Tire steering angle
α_{ij},σ_{ij}:	Slip angle and slip rate
$C_{\alpha_{ij}}$,$C_{\sigma_{ij}}$:	Cornering and longitudinal stiffness
$\rho_{x_{ij}}$,$\rho_{y_{ij}}$:	Long. and Lat. relaxation lengths
Ω_{ij}:	Wheel spin speed
$r_{w_{ij}}$:	Tire radius
$h_{z_{ij}}$:	Suspension length
t_s:	Sample period

*The authors acknowledge the grants: Ph.D. FAPESP (2014/06610-8), BEPE FAPESP (2014/27240-4) and Regular FAPESP Project VERDE (2014/02672-9). This work was carried out within the framework of the Equipex ROBOTEX (Reference ANR-10-EQPX-44-01) Heudiasyc Laboratory UMR CNRS UTC 7253.

[1]Rafael A. Cordeiro (Ph.D. student) and Paulo A. V. Ferreira are with the School of Electrical and Computer Engineering, University of Campinas, Campinas, Brazil: rcordeir@dt.fee.unicamp.br, valente@dt.fee.unicamp.br

[2]Alexandre M. Ribeiro (Ph.D. student) and José R. Azinheira are with the Instituto Superior Técnico, Universidade de Lisboa, Lisbon, Portugal: monteiroribeiro@tecnico.ulisboa.pt, jraz@dem.ist.utl.pt

[3]Alessandro C. Victorino is with the Heuristique et Diagnostic des Systèmes Complexes (HEUDIASYC), UMR CNRS 7253, Université de Technologie de Compiègne, Compiègne, France: Alessandro.Victorino@utc.fr

[4]Ely C. de Paiva is with the School of Mechanical Engineering, University of Campinas, Campinas, Brazil: elypaiva@fem.unicamp.br

[5]Samuel S. Bueno is with the Division of Robotics and Computer Vision, Center for Information Technology Renato Archer, Campinas, Brazil: samuel.bueno@cti.gov.br

I. INTRODUCTION

New technologies have been continuously developed in the automobile industry, creating the so called "intelligent vehicles". Most of these technologies are developed for ordinary passenger cars, prioritizing urban environments. More recently, all-terrain environments, in which vehicles are often traveling in uneven and slippery grounds with banked road profiles, have been considered. Intelligent all-terrain vehicles are still a challenging subject [1], but their applications are very promising in many areas, especially in surveillance, agriculture and rescue.

In intelligent vehicles there are two main classes of systems being developed: the Advanced Driver Assistance Systems (ADAS) and the Autonomous Vehicle (AV) systems. In ADAS, the main goal is to aid human drivers, acting direct or indirectly on the vehicle to enhance safety, comfort, *etc*. In the other hand, AV systems aim to substitute the human driver, controlling the entire vehicle.

To be able to make precise decisions, both ADAS and AV systems need to be fed with information related to driving activity. Therefore, they should be able to sense the vehicle dynamics, such as accelerations and forces. Moreover, the environment is also dynamic during driving, being these changes important to the AV decision-making problem, especially in all-terrain conditions.

There are several sensors that could be used to provide essential information for ADAS and AVs: accelerometer, gyrometer, video camera, laser, gps, *etc*. are default sensors in intelligent vehicles. However, there are some difficult variables to be measured. Furthermore, some sensors are expensive which prevents their use in ordinary passengers car. Among these variables, we have the road grade angles and Tire-Ground Interaction Forces (TGIFs).

In ADAS, for example, road angles and TGIFs can be used to predict rollover situations [2], allowing the system to warn, or even to act on the vehicle to avoid accidents. For AVs, they are extremely important for the off-road navigation problem [3], in which the terrain profile and adherence are dynamically changing, often leading to instability.

To obtain the desired information avoiding expensive sensors, estimators have been developed. Works as [4], [5], and [6] present estimators to measure tire forces, while [7] and [8] address the road grade estimation problem.

This work proposes a estimator for road grade angles and tire ground interaction forces based on a Delayed Interconnected (DI) cascade observer structure. A new approach

using a Two-Stage Extended Kalman Filter (TSEKF) [9] is proposed to estimate road grade angles along with all-directions tire forces in each wheel. The TSEKF is a interesting solution since it is a robust nonlinear estimation that allows the estimation of the road slopes, which has a very slow dynamics, along with the TGIFs.

This paper is organized as follows: The DI estimation structure is presented in section II. Then, two vehicle models are described in section III. These models are used to synthesize TSEKF and EKF observers in section IV. In section V, the proposed estimator is validated offline using real data acquired during a experiment in a banked proving ground. Final conclusions and future works are discussed in section VI.

II. DI ESTIMATION STRUCTURE

Complete vehicle dynamic models are very complex, therefore, their direct usage in estimation leads to extremely hard optimization problems or even to non observable solutions. Ray [4] and Doumiati *et al.* [6] proposed to decouple the problem by using cascade observer structure. However, to separate the models, both use random-walk models for the unknown decoupled dynamics. The delayed interconnected structure, proposed in [10] and shown in Fig. 1, allows model decoupling without using the random-walk models.

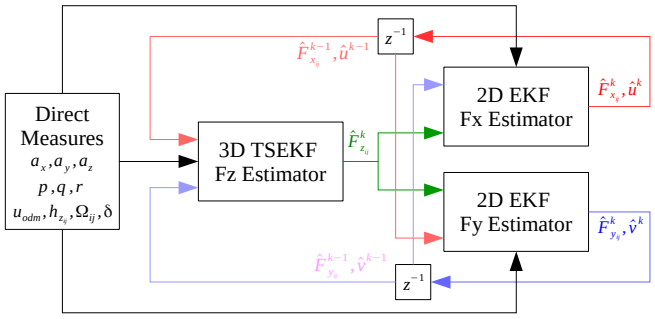

Fig. 1. Cascade-observer structure with delayed interconnections.

In the structure of Fig. 1, observers outputs are used as inputs or measurements in other observers of the cascade structure. To ensure the feasibility of the DI estimator, some outputs need to be delayed in time before being used for other observers. These interconnections are only possible because the delayed variables have slow dynamics in comparison to the sensors sample rate.

III. VEHICLE MODELS

This section briefly introduces the two nonlinear dynamic models used herein for observer synthesis: a 3D vehicle model is used by a vertical forces observer; a 2D yaw model is used for lateral and longitudinal TGIFs estimation. More details of the models can be found in [10].

A. 3D FULL-VEHICLE MODEL

The vertical forces observer is based on the 3D full-vehicle model represented in Fig. 2. The model considers a rigid planar body with four suspensions modeled as a spring-damper system, assumed vertical to the vehicle body. The tire masses are neglected, being represented by a single contact-point. A locally planar ground is assumed on each tire, enabling uneven ground profiles. Applying Newton-Euler dynamics equations, we obtain:

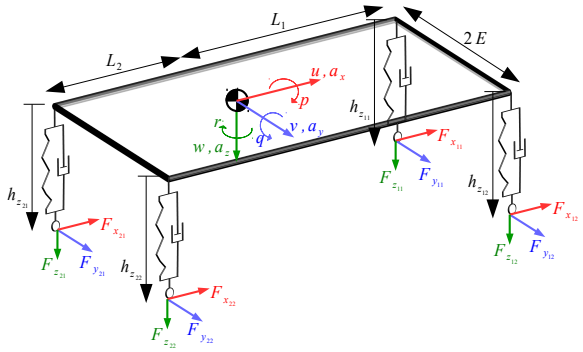

Fig. 2. Proposed 3D model for the vertical estimator.

$$\dot{u} = vr - wq - g\sin\theta + \frac{1}{m}\sum F'_{x_{ij}} \tag{1}$$

$$\dot{v} = wp - ur + g\sin\phi\cos\theta + \frac{1}{m}\sum F'_{y_{ij}} \tag{2}$$

$$\dot{w} = uq - vp + g\cos\phi\cos\theta + \frac{1}{m}\sum F_{z_{ij}} \tag{3}$$

$$\dot{p} = \frac{1}{J_{xx}}[(J_{yy} - J_{zz})\,qr - E(F_{z_{11}} + F_{z_{21}}) + E(F_{z_{12}} + F_{z_{22}}) - \sum h_{z_{ij}} F'_{y_{ij}}] \tag{4}$$

$$\dot{q} = \frac{1}{J_{yy}}[(J_{zz} - J_{xx})\,pr - L_1(F_{z_{11}} + F_{z_{12}}) + L_2(F_{z_{21}} + F_{z_{22}}) + \sum h_{z_{ij}} F'_{x_{ij}}] \tag{5}$$

$$\dot{r} = \frac{1}{J_{zz}}[(J_{xx} - J_{yy})\,pq + L_1(F'_{y_{11}} + F'_{y_{12}}) - L_2(F'_{y_{21}} + F'_{y_{22}}) + E(F'_{x_{11}} + F'_{x_{21}}) - E(F'_{x_{12}} + F'_{x_{22}})] \tag{6}$$

$$\dot{\phi} = p + (q\sin\phi + r\cos\phi)\tan\theta \tag{7}$$

$$\dot{\theta} = q\cos\phi - r\sin\phi \tag{8}$$

where:

$$\begin{bmatrix} F'_{x_{ij}} \\ F'_{y_{ij}} \end{bmatrix} = \begin{bmatrix} \cos\delta_{ij} & -\sin\delta_{ij} \\ \sin\delta_{ij} & \cos\delta_{ij} \end{bmatrix} \begin{bmatrix} F_{x_{ij}} \\ F_{y_{ij}} \end{bmatrix} \tag{9}$$

express the conversion of the horizontal forces from the tire frame to the vehicle frame.

Since the ground is locally planar, the derivative of the distances between the chassis extremities and the road ($\dot{h}_{z_{ij}}$) are equal to minus the vertical velocity of these extremities:

$$\dot{h}_{z_{ij}} = -w - (-1)^i qL_i - (-1)^j pE \tag{10}$$

Equations (1) to (10) represent a 12-states model. Defining $X_z = [u\ v\ w\ p\ q\ r\ \phi\ \theta\ \{h_{z_{ij}}\}_{1x4}]^T$ and $U_z = [\{F_{x_{ij}}\}_{1x4}\ \{F_{y_{ij}}\}_{1x4}\ \{\delta_{1j}\}_{1x2}]^T$, the model is:

$$\dot{X}_z = f_z(X_z, U_z) \tag{11}$$

The vertical forces can be reconstructed by computing the suspension forces using the states X_z and (10) in a linear spring-damper model:

$$\begin{aligned}\hat{F}_{z_{ij}} =& -k_s(\overline{h_{z_{ij}}} - \hat{h}_{z_{ij}}) - c_s(\hat{w} + (-1)^i \hat{q} L_i \\ &+ (-1)^j \hat{p} E)\end{aligned} \tag{12}$$

where $\overline{h_{z_{ij}}}$ is the theoretical relaxed suspension length.

B. 2D YAW MODEL

For lateral and longitudinal forces observation, the 2D yaw model represented in Fig. 3 is used. Also, a simplified Single Contact-Point Transient Model (SCPTM) [11] is implemented by describing the transient force as a first-order model – relaxation lengths are constants.

The application of Newton-Euler equations to the proposed 2D model provides:

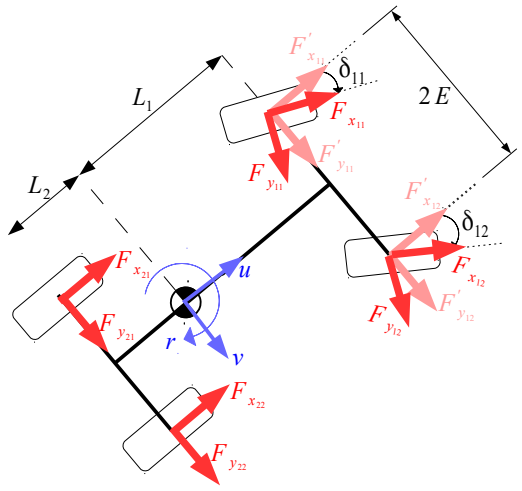

Fig. 3. 2D yaw dynamic model for longitudinal and lateral observers.

$$\dot{u} = vr + \frac{1}{m}\sum F'_{x_{ij}} \tag{13}$$

$$\dot{v} = -ur + \frac{1}{m}\sum F'_{y_{ij}} \tag{14}$$

$$\begin{aligned}\dot{r} =& \frac{1}{J_{zz}}[L_1\left(F'_{y_{11}} + F'_{y_{12}}\right) - L_2\left(F'_{y_{21}} + F'_{y_{22}}\right) \\ &+ E\left(F'_{x_{11}} - F'_{x_{12}}\right) - E(F'_{x_{12}} + F'_{x_{22}})]\end{aligned} \tag{15}$$

$$\dot{F}_{d_{ij}} = \frac{u - (-1)^j r}{E\rho_{d_{ij}}}\left(\overline{F_{d_{ij}}} - F_{d_{ij}}\right) \tag{16}$$

where d corresponds to x for the longitudinal estimator and y for the lateral.

The SCPTM is a function of the instantaneous forces $\overline{F_{d_{ij}}}$ at each tire. There are several tire force models in the literature [11], [12]. However, to allow real-time implementations, the Dugoff tire model [13] is adopted due to its simple nonlinear modeling and fast computing. In this model, the forces are obtained by:

$$\begin{aligned}\overline{F_{d_{ij}}} &= -C_{\tau_{ij}}\tau_{ij}\left(2 - \chi_{d_{ij}}\right)\chi_{d_{ij}} \\ \chi_{d_{ij}} &= \min\left\{1, \frac{\mu F_{z_{ij}}}{2C_\tau|\tau_{ij}|}\right\}\end{aligned} \tag{17}$$

where τ represents the slip ratio σ in the longitudinal model ($d = x$) and the sideslip angle α in the lateral model ($d = y$).

Two 7-states models are obtained using (13) to (16):

$$\dot{X}_x = f_x(X_x, U_x) \tag{18}$$

$$\dot{X}_y = f_y(X_y, U_y) \tag{19}$$

In these state-space models, $X_x = [u\ v\ r\ \{F_{x_{ij}}\}_{1x4}]^T$ and $X_y = [u\ v\ r\ \{F_{y_{ij}}\}_{1x4}]^T$ are the states and $U_x = [\{F_{y_{ij}}\}_{1x4}\ \{F_{z_{ij}}\}_{1x4}\ \{\Omega_{ij}\}_{1x4}\ \{\delta_{1j}\}_{1x2}]^T$ and $U_y = [\{F_{x_{ij}}\}_{1x4}\ \{F_{z_{ij}}\}_{1x4}\ \{\delta_{1j}\}_{1x2}]^T$ are the inputs.

IV. TSEKF AND EKF OBSERVERS

The models described in section III are used to synthesize observers assembled in the DI cascade structure. In all-terrain environments, vehicle are often traveling in sloped terrains. To account for that, this work proposes the use of a Two-Stage Extended Kalman Filter [9] to estimate the road grades along with the vertical tire forces acting on each wheel.

Considering roll and pitch angles as the sum of the vehicle body angles (ϕ_V and θ_V) and the road grade angles (ϕ_R and θ_R), we can rewrite (7) and (8) as:

$$\dot{\phi}_V = p + [q\sin\phi + r\cos\phi]\tan\theta - \dot{\phi}_R \tag{20}$$

$$\dot{\theta}_V = q\cos\phi - r\sin\phi - \dot{\theta}_R \tag{21}$$

Thus, substituting $\phi = \phi_V + \phi_R$ and $\theta = \theta_V + \theta_R$ in (11) and using (20) and (21) instead of (7) and (8), the model now has ϕ_V and θ_V as states, and $\Gamma = [\phi_R\ \theta_R]^T$ is considered an unknown input to be estimated by the TSEKF. The unknown derivatives $\dot{\phi}_R$ and $\dot{\theta}_R$ are included in the process noise. Using a direct Euler discretization, the system can be rewritten as a discrete stochastic model:

$$\begin{cases} X_{k+1} = X_k + t_s f(X_k, U_k, \Gamma_k) + W_k \\ \qquad \approx A_k X_k + F_k \Gamma_k + W_k \\ \Gamma_{k+1} = \Gamma_k + \Lambda_k \\ Y_k = h(X_k, U_k, \Gamma_k) + V_k \\ \qquad \approx C_k X_k + G_k \Gamma_k + V_k \end{cases} \tag{22}$$

where:

$$\begin{aligned} A_k &= I + t_s \nabla_X f(X, U, \Gamma)\Big|_{X=X_k,\, U=U_k,\, \Gamma=\Gamma_k} \\ C_k &= \nabla_X h(X, U, \Gamma)\Big|_{X=X_k,\, U=U_k,\, \Gamma=\Gamma_k} \\ F_k &= I + t_s \nabla_\Gamma f(X, U, \Gamma)\Big|_{X=X_k,\, U=U_k,\, \Gamma=\Gamma_k} \\ G_k &= \nabla_\Gamma h(X, U, \Gamma)\Big|_{X=X_k,\, U=U_k,\, \Gamma=\Gamma_k} \end{aligned}$$

The process noises W and Λ, and the measurement noise V are assumed to be uncorrelated white noises: $E\{W\} =$

$E\{\Lambda\} = E\{V\} = 0$, $E\{WW^T\} = Q^X$, $E\{\Lambda\Lambda^T\} = Q^\Gamma$ and $E\{VV^T\} = R$, where Q^X, Q^Γ and R are diagonal matrices, as noise channels are assumed uncorrelated.

With (22), it is possible to apply the TSEKF algorithm described in [9]:

1) Prediction:

$$\begin{cases} \hat{X}_{k+1|k} = \hat{X}_{k|k} + t_s f(\hat{X}_{k|k}, U_k, \hat{\Gamma}_{k|k}) \\ \hat{\Gamma}_{k+1|k} = \hat{\Gamma}_{k|k} \\ \hat{P}^\Gamma_{k+1|k} = \hat{P}^\Gamma_{k|k} + Q^\Gamma \end{cases} \tag{23}$$

2) Bias-free state estimation:

$$\begin{cases} r_k = A_k \beta_{k|k} + F_k \\ \beta_{k+1|k} = r_k \hat{P}^\Gamma_{k|k} (\hat{P}^\Gamma_{k+1|k})^{-1} \\ \tilde{X}_{k+1|k} = \hat{X}_{k+1|k} - \beta_{k+1|k} \hat{\Gamma}_{k+1|k} \\ \tilde{P}^X_{k+1|k} = A_k \tilde{P}^X_{k|k} A_k^T + Q^X + r_k \hat{P}^\Gamma_{k|k} r_k^T \\ \qquad - \beta_{k+1|k} \hat{P}^\Gamma_{k+1|k} \beta^T_{k+1|k} \\ \eta^X_k = Y_m - C_k \tilde{X}_{k+1|k} - h(\hat{X}_{k+1|k}, U_k, \hat{\Gamma}_{k+1|k}) \\ \qquad + C_k \hat{X}_{k+1|k} + G_k \hat{\Gamma}_{k+1|k} \\ K^X_k = \tilde{P}^X_{k+1|k} C_k^T (C_k \tilde{P}^X_{k+1|k} C_k^T + R)^{-1} \\ \tilde{X}_{k+1|k+1} = \tilde{X}_{k+1|k} + K^X_k \eta^X_k \\ \tilde{P}^X_{k+1|k+1} = (I - K^X_k C_k) \tilde{P}^X_{k+1|k} \end{cases} \tag{24}$$

3) Bias estimation:

$$\begin{cases} H_k = G_k + C_k \beta_{k+1|k} \\ \beta_{k+1|k+1} = \beta_{k+1|k} + K^X_k H_k \\ \eta^\Gamma_k = Y_m - h(\hat{X}_{k+1|k}, U_k, \hat{\Gamma}_{k+1|k}) \\ K^\Gamma_k = \tilde{P}^\Gamma_{k+1|k} H_k^T (H_k \tilde{P}^\Gamma_{k+1|k} H_k^T \\ \qquad + C_k \tilde{P}^X_{k+1|k} C_k^T + R)^{-1} \\ \hat{\Gamma}_{k+1|k+1} = \hat{\Gamma}_{k+1|k} + K^\Gamma_k \eta^\Gamma_k \\ \hat{P}^\Gamma_{k+1|k+1} = (I - K^\Gamma_k H_k) \tilde{P}^\Gamma_{k+1|k} \end{cases} \tag{25}$$

4) Bias correction

$$\begin{cases} \hat{X}_{k+1|k+1} = \tilde{X}_{k+1|k+1} + \beta_{k+1|k+1} \Gamma_{k+1|k+1} \\ \hat{P}^X_{k+1|k+1} = \tilde{P}^X_{k+1|k+1} + \beta_{k+1|k+1} \hat{P}^\Gamma_{k+1|k+1} \end{cases} \tag{26}$$

For longitudinal and lateral force observers, the standard EKF filter is applied using the 2D yaw dynamic model, as in [10].

The measurement vector and the noise correlation matrices for each observer are:

- Vertical observer:

$$Y_z = \left[a_x \; a_y \; a_z \; p \; q \; r \; \overline{\phi} \; \overline{\theta} \; h_{z_{11}} \; h_{z_{12}} \; h_{z_{21}} \; h_{z_{22}} \; \hat{u} \; \hat{v}\right]^T$$
$$Q_z^X = 0.01\text{diag}\left([1\ 1\ 1\ 0.1\ 0.1\ 0.1\ 1\ 1\ 1\ 1\ 1\ 1]\right)$$
$$Q_z^\Gamma = \text{diag}\left([0.001\ 0.001]\right)$$
$$R_z = 0.01\text{diag}\left([1\ 1\ 1\ 5\ 5\ 5\ 10\ 10\ 10\ 10\ 10\ 10\ 10\ 10]\right)$$

- Lateral observer:

$$Y_y = [a_x \; a_y \; r \; \hat{u}]^T$$
$$Q_y = \text{diag}\left([0.01\ 0.01\ 0.001\ 1\ 1\ 1\ 1]\right)$$
$$R_y = \text{diag}\left([0.1\ 0.1\ 0.05\ 0.1]\right)$$

- Longitudinal observer:

$$Y_x = [a_x \; a_y \; r \; u_{odm} \; \hat{v}]^T$$
$$Q_x = \text{diag}\left([0.01\ 0.01\ 0.001\ 1\ 1\ 1\ 1]\right)$$
$$R_x = \text{diag}\left([0.1\ 0 - 1\ 0.05\ 0.10.1]\right)$$

The outputs u_{odm}, a_x, a_y, a_z, p, q, r and $h_{z_{ij}}$ are direct measures of the vehicle, $\overline{\phi}$ and $\overline{\theta}$ are pseudo-measures, obtained as in (27) and (28) using the suspension displacement, while $\hat{u}$ and $\hat{v}$ are delayed outputs of the longitudinal and lateral force observers, respectively.

$$\overline{\phi} = \frac{h_{z_{11}} - h_{z_{12}} + h_{z_{21}} - h_{z_{22}}}{4E} \tag{27}$$

$$\overline{\theta} = \frac{h_{z_{11}} - h_{z_{21}} + h_{z_{12}} - h_{z_{22}}}{2L_1 + 2L_2} \tag{28}$$

V. EXPERIMENTAL VALIDATION

To validate the proposed estimators, real data was obtained from the vehicle platform DYNA (DYNamics Analysis), shown in Fig. 4.

Fig. 4. Dyna testbed platform.

Heudiasyc lab uses the platform DYNA as testbed for dynamics studies and models validation [6], [8]. The platform is fully equipped: a Crossbow IMU provides accelerations a_x, a_y and a_z, and angular speeds p, q and r; four Corrsys laser sensors measure heights $h_{z_{ij}}$ between the chassis and the ground near the tires, which are also used to calculate $\overline{\phi}$ and $\overline{\theta}$; and vehicle odometry gives u_{odm}. Additionally, the platform has four Kistler RoaDyn tire forces transducers to be used as ground truth for the estimators.

A mission was held in the UTAC CERAM proving ground, in Mortefontaine, France (see Fig. 5). For safety reasons, the first experiment was not held in a all-terrain environment, but it will be performed in the near future. The trajectory corresponds to an oval circuit with three different banked lanes (15^o, 30^o and 40^o), as seen in Fig. 5(b).

In the mission, accomplished by a professional driver, a slalom maneuver was made in the banked lanes. Fig. 6 shows the speed and the steering of the vehicle during the interval between $80s$ and 140s, represented in blue in Fig. 5(a).

(a) (b)

Fig. 5. Mission at UTAC CERAM: (a) trajectory; (b) banked road.

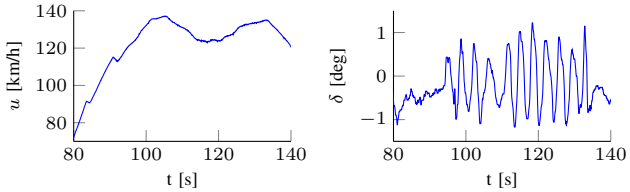

(a) Long. speed (b) Steering

Fig. 6. Vehicle speed and steering angle during mission.

The data were acquired by the sensors in a sample rate of 100 Hz and used offline to feed the estimator, implemented in MATLAB/SIMULINK. Fig. 7 presents the measured tire forces and estimations using the EKF from [10] and the TSEKF for the front-left and the rear-right tires.

The estimated forces are consistent with the real data. The lateral and vertical tire forces are near to their expected values, even during the slalom maneuver, when the forces are stronger and change rapidly. For the longitudinal forces estimation, there is an unexpected bias error in the measured longitudinal forces in rear non-motorized tires, as their mean values should be closer to zero. Even so, the estimated errors in the longitudinal force are larger, mostly due to the difficulty of estimating slip ratios.

Comparing EKF and TSEKF results, there is no substantial improvement in using the TSEKF. With the hypothesis of locally planar terrain with different cotes in each wheel, the banked road is already considered by the EKF. To better compare the estimators, a normalized error is proposed:

$$err = 100 \times \frac{|\hat{F}_{ij} - F_{ij}|}{\max_{i,j} F_{ij}} \tag{29}$$

This error is computed for all forces between 80s and 140s. In Fig. 8, histograms are presented for vertical lateral and longitudinal forces combining every tire. The sample errors are distributed in the intervals: a) 0 to 1%; b) 1% to 3%; c) 3% to 5%; d) 5% to 7%; e) 7% to 9%; f) 9% to 11%; g) 11% to 13%; h) 13% to 15%; and i) greater than 15%. The histograms show that, for all force directions, there are more samples with low errors (intervals a, b and c) using the TSEKF instead of the EKF. It can be noted that there is a large number of samples with error greater than 15%

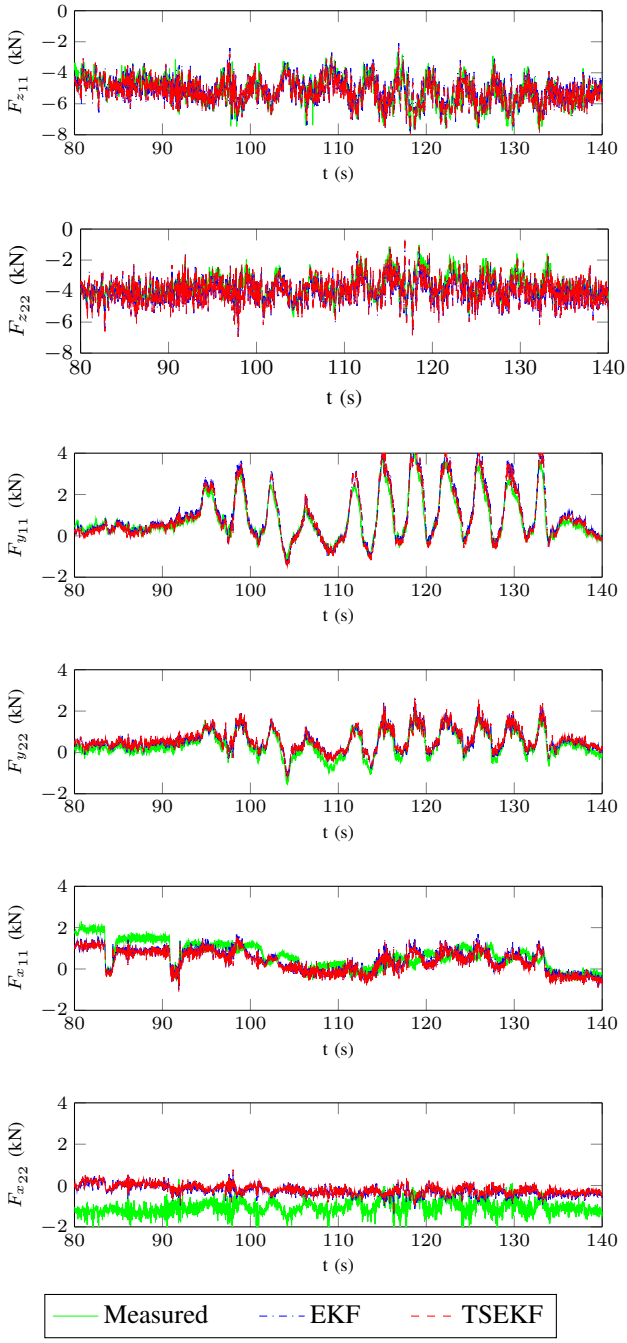

Fig. 7. Estimated vertical, lateral and longitudinal forces on the front-left and rear-right tires.

(interval i) in the x direction, which is a direct consequence of the bias error in the rear wheels, as discussed above.

Also, as discussed in [10], the slip ratio is a normalized quantity of the difference between the longitudinal speed of the wheel and their expected velocity calculated from the wheel spin speed. As the only speed measurement is obtained from the odometer, there is a direct correlation between the estimated linear velocity of the wheel and its spin speed. Moreover, the calculated velocity based on the wheel spin speed is a function of the tire radius, which changes with

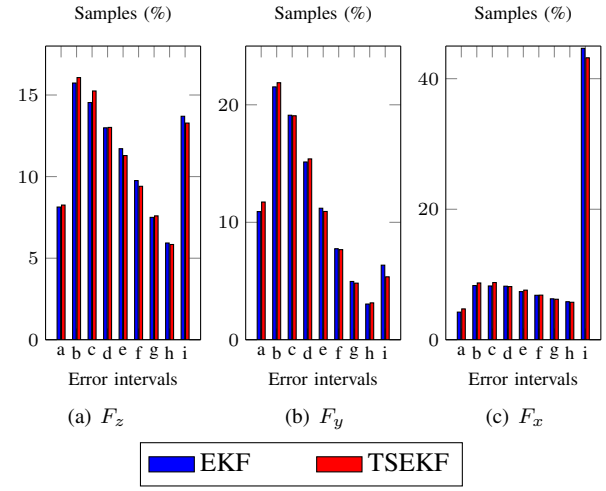

Fig. 8. Distributiom of the normalized estimation error for each sample measure.

the vertical forces distribution, representing another source of error in the longitudinal force estimation.

Finally, the TSEKF estimation of the road grade angles are shown in Fig. 9. The results are compared with the ones obtained using a Recursive Least-Square (RLS) approach presented by Jiang *et al.* [8].

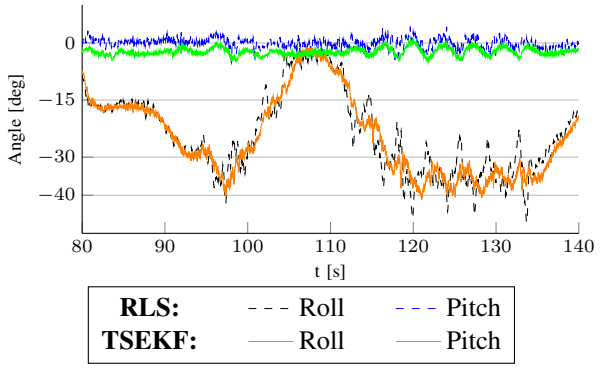

Fig. 9. Estimated road grade angles.

Note that, in the interval between 80 and 90 seconds, the vehicle is traveling along the 15^o and 30^o lanes. Also, the TSEKF estimated grade never goes up to 40^o, which is the maximum slope of the road. Since the oval circuit is performed counter-clockwise, the roll angle is negative, which is expected for the North-East-Down referential system used in the models described in section III. Comparing the TSEKF results with the angles obtained using the RLS algorithm, the TSEKF is less sensible to the dynamics variations, especially during the slalom maneuver, producing a more reasonable estimation of the road grade.

VI. Conclusion

This work presented an implementation of a Two-Stage Extended Kalman Filter in order to estimate road grades, along with TGIFs, during a vehicle mission. The TSEKF was implemented as a vertical tire force observer, which is part of a delayed interconnected cascade observer structure. The results obtained with the TSEKF show to be consistent with the road information of the UTAC CERAM proving ground, and also robust to variations and errors in the force estimators.

The estimated tire-ground forces are similar to the measure ones, even during slalom maneuver in a banked road. The longitudinal force estimation is better in the motorized wheels since the slip ratios are bigger in these wheels. Also, the acceleration reconstructed with the estimated forces are very similar to the measures from the IMU, indicating that the estimated TGIFs describe correctly the vehicle dynamics.

Future work will include torque information in motorized wheels and in the electrical steering system in order to enhance TGIFs estimation. Also, the TSEKF technique will be used to estimate friction coefficients in each tire, making the estimator suitable tool for all-terrain vehicles.

References

[1] T. Luettel, M. Himmelsbach, and H. J. Wuensche, "Autonomous ground vehicles – concepts and a path to the future," *Proceedings of the IEEE*, vol. 100, no. Special Centennial Issue, pp. 1831–1839, May 2012.

[2] N. Bouton, R. Lenain, B. Thuilot, and P. Martinet, "A rollover indicator based on a tire stiffness backstepping observer: Application to an all-terrain vehicle," in *Intelligent Robots and Systems, 2008. IROS 2008. IEEE/RSJ International Conference on*, Sept 2008, pp. 2726–2731.

[3] E. Lucet, R. Lenain, and C. Grand, "Dynamic path tracking control of a vehicle on slippery terrain," *Control Engineering Practice*, vol. 42, pp. 60 – 73, 2015.

[4] L. R. Ray, "Nonlinear tire force estimation and road friction identification: Simulation and experiments1,2," *Automatica*, vol. 33, no. 10, pp. 1819 – 1833, 1997.

[5] N. K. M'sirdi, A. Rabhi, N. Zbiri, and Y. Delanne, "Vehicle-road interaction modelling for estimation of contact forces," *Vehicle System Dynamics*, vol. 43, no. sup1, pp. 403–411, 2005.

[6] M. Doumiati, A. Victorino, A. Charara, and D. Lechner, "Onboard real-time estimation of vehicle lateral tire-road forces and sideslip angle," *Mechatronics, IEEE/ASME Transactions on*, vol. 16, no. 4, pp. 601–614, Aug 2011.

[7] I. Kim, H. Kim, J. Bang, and K. Huh, "Development of estimation algorithms for vehicle's mass and road grade," *International Journal of Automotive Technology*, vol. 14, no. 6, pp. 889–895, 2013.

[8] K. Jiang, A. C. Victorino, and A. Charara, "Real-time estimation of vehicle's lateral dynamics at inclined road employing extended kalman filter," in *11th IEEE conference on Industrial Electronics and Applications (ICIEA 2016)*, Hefei, China, June 2016.

[9] X. Chen, R. Sun, W. Jiang, Q. Jia, and J. Zhang, "A novel two-stage extended kalman filter algorithm for reaction flywheels fault estimation," *Chinese Journal of Aeronautics*, vol. 29, no. 2, pp. 462 – 469, 2016.

[10] R. A. Cordeiro, A. C. Victorino, P. A. Ferreira, E. C. de Paiva, and S. S. Bueno, "Tire-ground forces estimation in a 4-wheel vehicle using a delayed interconnected cascade-observer structure*," *IFAC-PapersOnLine*, vol. 49, no. 15, pp. 139 – 144, 2016, 9th {IFAC} Symposium on Intelligent Autonomous Vehicles {IAV} 2016, Leipzig, Germany, 29 June - 1 July 2016.

[11] H. B. Pacejka, *Tire and Vehicle Dynamics*. Oxford: Butterworth-Heinemann, 2002, 697p.

[12] G. Rill, *Road Vehicle Dynamics: Fundamentals and Modeling*, ser. Ground Vehicle Engineering Series. Taylor & Francis, 2011, 361p.

[13] H. Dugoff, P. S. Fancher, and L. Segal, "Tire performance characteristics affecting vehicle response to steering and braking control inputs," Office of Vehicle Systems Research, US National Bureau of Standards, Washington, DC, Tech. Rep. Contract CST-460 (Final), August 1969.